Design, Implementation, Control and Performance Analysis of Coupled Inductor Ćuk Converter

A THESIS SUBMITTED TO

THE FACULTY OF THE GRADUATE SCHOOL OF

THE UNIVERSITY OF MINNESOTA

BY

Anushree Ramanath

IN PARTIAL FULFILLMENT OF THE REQUIREMENTS

FOR THE DEGREE OF

MASTER OF SCIENCE

Adviser: Dr. Ned Mohan

April, 2020

Acknowledgements

I am indebted to my advisor, Dr. Ned Mohan for his constant support, enthusiasm, and mentoring without which this work would not have been complete. I extend my heartfelt thanks to Dr. William Robbins and Dr. Maria Gini for agreeing to be part of the committee and for being extremely supportive.

My sincere thanks to the support from the Research and Development Foundation (RDF) for enabling this research effort.

Thanks to all my friends, colleagues, and well-wishers for all the help through the process. Special thanks to everyone in my research lab for all the stimulating discussions and technical guidance.

Thanks to my parents for their everlasting encouragement.

Dedication

Dedicated to my dearest parents and all my teachers.

Abstract

Rooftop solar is becoming a popular source of energy for electricity generation. An optimal photovoltaic interface has ripple-free terminal currents and compact system design along with a high step-up ratio. Ćuk converter is a variant of the standard buck-boost converter. It is a great choice for integrating renewable energy sources due to its wide operating range and unique quality of continuous current flow at both the terminals. This drastically reduces the need for passive filters, system noise, and possible electromagnetic interference issues. With the use of a single coupled inductor instead of two separate inductances, the Ćuk converter can be designed to operate with ripple-free input or output current. However, only a minority of the users easily adapt Ćuk converter and its variants for their needs due to the complications in terms of the design method and absence of a rational design strategy for obtaining the suitable magnetics design that yields 'zero-ripple' terminal currents.

This thesis presents an innovative, definitive method with an analytical basis for determining the component values that cater to a broad range of applications for a coupled inductor Ćuk converter topology and contrasts it with the conventional Ćuk converter. This approach can be drawn out to work on other crucial converter topologies with integrated magnetics. The descriptive analysis is carried out with the aid of the MATLAB scripts developed and the theoretical results are validated with the help of simulation models created using the PLECS software platform. Magnetic design and equivalent modeling is carried out using ANSYS and the designed converter has been

implemented for experimental validation. Traditionally, the control of the Ćuk converter has been extremely complicated. For the chosen topology, control techniques have been investigated and performance analysis is carried out on a system level.

Table of Contents

List of Tables

List of Figures

Chapter 1

Introduction

DC-DC converters are utilized in several key systems including solar energy conversion systems, wind energy conversion systems, storage systems powered by batteries, and so on. The performance metrics like enhanced efficiency and very low ripple current in the input current makes it the popular choice. The on-going research in this area includes the study of non-isolated, isolated, symmetrical and asymmetrical converters and it targeted towards achieving reduced input current ripple, superior transient performance, steady-state stability and significant increase in the system efficiency [1]. In comparison with other classical converters, Ćuk converter is well-known for its capability to offer the ripple reduction in terminal currents which can be utilized for either step-up or step-down applications. Ćuk converter also offers important abilities such as continuous input current, buck-boost capability, and capacitive isolation between the source and the load [2] [3] [4].

1.1 Integration of Renewables

The topic of integration of renewables with the grid and storage has been of utmost importance in the recent years. Owing to the need for increasing zero net energy buildings and combating the rising effects of the climate crisis, there is no better alternative

than the use of renewable energy sources. A DC-DC converter with voltage step-up and step-down capabilities is desired due to the need for grid integration and storage. Isolation is not mandatory considering photovoltaic applications at the panel level. In this case, the ripple-free input current is essential for the efficient operation of the system. Conventional buck-boost converter possesses the required step-up and step-down capabilities. However, its current waveforms are not necessarily ripple-free and are pulsating in nature. This implies that the variants of the classical buck-boost converter like SEPIC and Ćuk converters are the possible preferences for the set of requirements. Both of these topologies aid in providing the suitable input current waveform by means of the input inductor present. However, a variant of the conventional Ćuk converter called the coupled inductor Ćuk converter yields close to ripple-free input current when designed appropriately.

1.2 Need for DC-DC Converters

DC-DC converters are used in renewable energy systems for enhancing the performance due to its innate qualities of high voltage gain, wide operating range, and reduced losses. There are several types of DC-DC converters [5]. They can be classified based on isolation capability as isolated and non-isolated DC-DC converters. Non-isolated converter topologies include the traditional buck, boost, buck-boost, Ćuk and SEPIC converters. The isolated converter topologies are flyback, forward, isolated half or full bridge and Ćuk with integrated magnetics [6]. The isolated versions of the converter typically contain a transformer in its topology leading to increased size and cost. However, when designed accurately, it can be used to facilitate either buck or boost operation and some variants with integrated magnetics have proven to be extremely cost-effective and compact as well.

1.3 State-of-the-Art

Boost converters are generally used for PV integration due to its ease of design and less number of components. Nonetheless, the major pain points with this topology are high conduction losses which lead to reduced efficiency and demand larger input inductor to achieve lower ripple in the input current [7]. Also, dealing with a large voltage ratio is not possible in boost configuration as the duty ratio approaches unity. This scenario leads to increased parasitic losses and demands high-resolution control.

A full-bridge converter has also been employed as an isolated topology for PV applications. However, the downside of incorporating this converter include large cost, lower reliability and reduced power density because of additional power stages and other components [8].

Resonant converters are another frequently used topology for implementing converters with high power density. They have the ability to operate at high switching frequencies with natural zero-voltage switching. But, they suffer from low controllability, complicated design process, and reduced efficiency at partial loads [9].

1.4 Outline and Contributions of the Thesis

- Analytical basis for design of coupled inductor Ćuk converter.
- Detailed design and parameter estimation of coupled inductor Ćuk converter for photovoltaic applications.
- Equivalent modeling and co-simulation of the electrical and magnetic components.
- Hardware prototype to experimentally validate the theoretical analysis and simulation results.

- Controller design for coupled inductor Ćuk converter.
- Loss analysis for coupled inductor Ćuk converter and comparison with the conventional Ćuk converter topology.
- System-level performance analysis of coupled inductor Ćuk converter.
- Study related to IEEE 1547 regulations for residential applications.

Chapter 2

Coupled Inductor

When two inductors are wound on the same magnetic core, a coupled inductor is formed. It is similar to a transformer except for the fact that the magneto-motive forces (MMFs) of the windings are additive in nature.

2.1 Motivation and Rationale

The design of magnetic components in converters is as important as the other electrical parameters and even slight enhancement in magnetic components can directly improve the overall design of the converter.

Two individual magnetic devices can be wound on a single magnetic core when their voltage waveforms are the same. This is as demonstrated in Fig. 2.1 and is the basis for obtaining ripple-free current on one of the terminals. The merits of coupling include the reduction in size and weight along with enhanced performance. In the case of separate inductor windings, there is no flow of AC flux in the center branch while the DC fluxes add up. However, the air gap between the two windings has to be increased to maintain linear behavior.

In the case of conventional Ćuk converter, identical voltage waveforms appear across both the inductors. Thus, the effective AC flux in the center branch is zero and can be

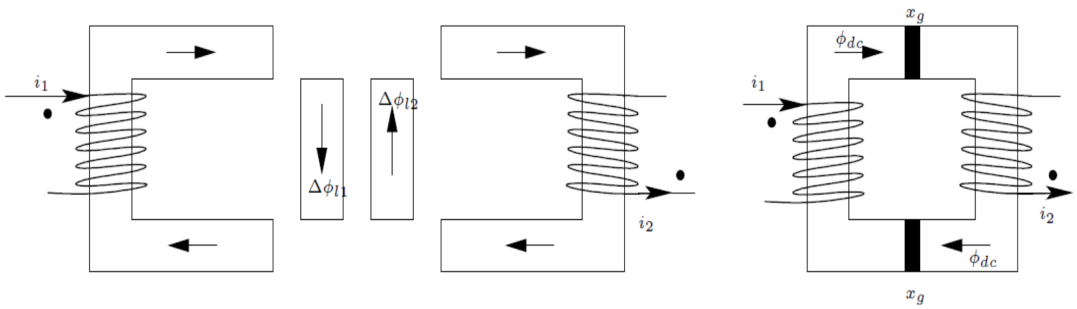

Figure 2.1: Two individual inductances forming a coupled inductor

removed. This yields a compact and magnetic component of less weight while maintaining the value of power density. Thus, there are no additional core losses which leads to increased efficiency.

The maximum voltages that can be obtained without saturation on the primary and secondary windings in case of a coupled inductor are:

$$V_1 = 4N_1 B_{max} S f_s \tag{2.1}$$

$$V_2 = 4N_2 B_{max} S f_s \tag{2.2}$$

where N_1 is the number of primary turns, B_{max} is the maximum flux density in the core, S is the cross-section and N_2 is the number of turns in the secondary winding.

The window area, W is said to be totally used up when:

$$kW = \frac{1}{J}(N_1 I_1 + N_2 I_2) \tag{2.3}$$

where k is the empirical fill factor of the windings and J is the current density in the windings.

Thus, the power handling capacity of the magnetic structure is given by:

$$P = VI \propto kWS \propto l^4 \tag{2.4}$$

where l is the linear dimension of the core.

This yields the following condition, also referred to as the magnetic scaling law:

$$Volume, Weight \propto l^3 \propto P^{\frac{3}{4}} \tag{2.5}$$

It is evident from (2.5) that the volume or weight of a magnetic device increases slower than its power handling capacity. This means that the power density is larger when the total power being processed is high. Thus, the use of a single, large power processing magnetic device is much better than using multiple smaller ones. A significant boost in power density can be realized by integrating several individual magnetic components.

2.2 Mutual Inductance

We know that the self-inductance of an inductor with N turns is given by:

$$L = \frac{N\phi}{I} = \frac{\mu_0 N^2 A}{l} \tag{2.6}$$

where ϕ is the magnetic flux through one turn of the solenoid due to the magnetic field produced by I.

When two coils are placed close to each other, a portion of the flux induced by the current through the second winding is linked to the first winding as is known as mutual flux. The remainder of the flux is called the residual or leakage flux of the other winding. This implies that the voltage on the first winding depends on the rate of change of flux. Mutual inductance is the interaction of one coil's magnetic field on another coil as it induces a voltage in the adjacent coil. In terms of the self inductances of the coils,

mutual inductance can be represented as:

$$M = \sqrt{L_1 L_2} \tag{2.7}$$

In general, mutual inductance is represented as

$$M = k\sqrt{L_1 L_2} \tag{2.8}$$

where k is the coupling coefficient given by $0 \leq k \leq 1$. Typically, k is used as a measure of tightness when two inductors are coupled (leakage flux is zero). This also translates to the fact that mutual inductance is zero if inductor are not coupled as k = 0.

2.3 Ripple-steering Phenomenon

This phenomenon is generic in nature and can be incorporated in any switching converter where the coupled inductor technique is advantageous. It is an AC phenomenon (meaning, it is independent of the DC operating point of the switching converter). It can be employed even during no-load conditions and functions amidst non-idealities. Consider the case of a two-winding inductor. The following equations can be obtained [10]:

$$v_1 = L_{11}\frac{di_1}{dt} + L_M\frac{di_2}{dt} = (L_{11} - L_M)\frac{di_1}{dt} + L_M\frac{d}{dt}(i_1 + i_2) \tag{2.9}$$

$$v_2 = L_M\frac{di_1}{dt} + L_{22}\frac{di_2}{dt} = (L_{22} - L_M)\frac{di_2}{dt} + L_M\frac{d}{dt}(i_1 + i_2) \tag{2.10}$$

From Fig. 2.2 (typically referred to as T-model), we have:

$$v_1 = (L_{11} - \frac{L_M}{A})\frac{di_1}{dt} + \frac{L_M}{A}\frac{d}{dt}(i_1 + Ai_2) \tag{2.11}$$

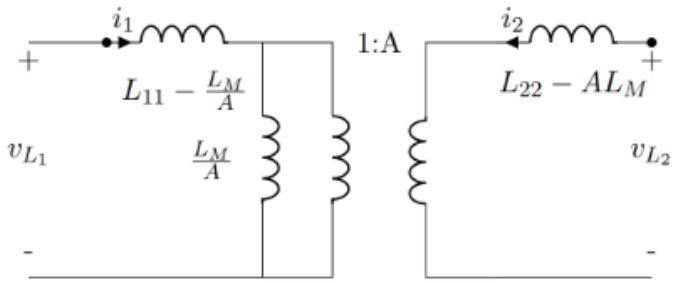

Figure 2.2: Ripple steering phenomenon

$$v_2 = (L_{22} - AL_M)\frac{di_2}{dt} + AL_M\frac{d}{dt}(\frac{i_1}{A} + i_2) \tag{2.12}$$

where L_M is the magnetizing inductance. It is ideal to choose the value of A to be equal to the physical turns ratio, $\frac{N_2}{N_1}$ as it can closely match the characteristics of the physical device. This can be referred to as the physical model due to its close resemblance to the actual physical structure.

Chapter 3

Converter Design

3.1 Objectives Addressed

The choice and design of appropriate converters are inevitable for many applications including integration of renewables, storage systems, electric vehicles and so on. The primary idea behind the design aspects discussed is to focus on residential-scale photovoltaic (PV) applications or rooftop solar installations. Fig. 3.1 depicts the overall setup and the component of focus for the current research endeavor.

The major objectives addressed include improved efficiency, zero-ripple input current, and low part count to achieve weight reduction, efficient control strategies, and plug-and-play capability. Also, other performance metrics like reduced electromagnetic interference (EMI), elimination of huge capacitor at the input side and the use of high-bandwidth controller. The designed converter is ideal for incorporating multiple sources or loads for a wide range of nominal voltages.

3.2 Ćuk Converter

The Ćuk converter is a modification of the typical buck-boost converter. It is known for increasing or decreasing the resultant voltage in comparison with the voltage at the

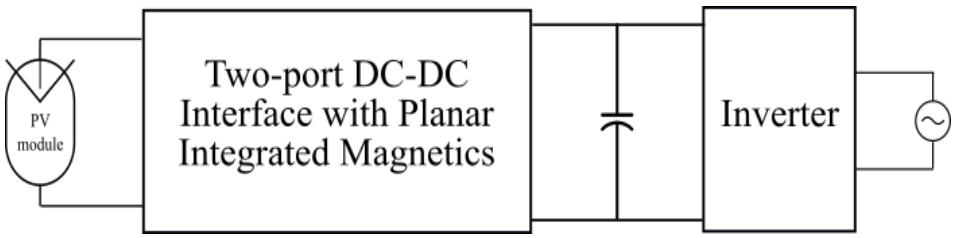

Figure 3.1: Block representation of DC-DC converter interfaced with PV

input terminal depending on the specifications. Zero-ripple terminal currents can be attained and adjustments to the conventional topology can be made to realize better non-pulsating current waveforms. The circuit diagram of a conventional Ćuk converter is shown in Fig. 3.2.

The analysis of the circuit is presented considering the converter operates in continuous conduction mode (CCM). This comprises of two separate intervals of time which can be expressed as Mode 1 and Mode 2 of converter operation. In mode 1, the switch is conducting and the diode is not conducting. In mode 2, the diode is in ON state and the switch is in OFF state. Kirchoff's voltage and current laws are utilized in the process of analyzing the circuit. The nuances of operation of this conventional converter is well articulated in literature [11].

It is key to observe that the input voltage is constant and voltage at the output is also essentially constant considering the voltage ripple to be negligible. When the inductors L_1 and L_2 are coupled and wound on the same core, coupled inductor Ćuk converter topology can be obtained.

3.2.1 Analysis of the Basic Topology

The analytical equations for standard Ćuk converter topology are pretty direct [11]. By utilizing them, estimation of the necessary parameters can be accomplished as highlighted in [12]. To be able to facilitate comparison with other advanced topologies, the conditions essential for the design of the Ćuk converter are summarized below:

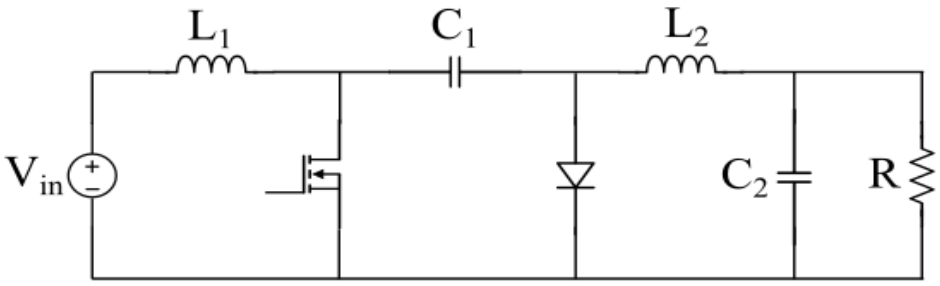

Figure 3.2: Conventional Ćuk converter

$$\frac{v_o}{v_{in}} = \frac{D}{1-D} = \frac{t_{on}}{t_{off}} \tag{3.1}$$

where V_o is the output voltage, V_{in} is the input voltage, D is the duty cycle, t_{on} is the on period and t_{off} is the off period. The value of D can be computed given the input and output voltages using (3.1). The total time interval, T_s is the inverse value of the switching frequency of the converter, f_{sw}.

The output current, I_o and load resistance, R can be calculated using the output power and output voltage as in (3.2) and (3.3).

$$I_o = \frac{P_o}{V_o} \tag{3.2}$$

$$R = \frac{{V_o}^2}{P_o} \tag{3.3}$$

Further, inductances L_1 and L_2, and capacitances C_1 and C_2 can be conveniently calculated using (3.4) and (3.5).

$$L_1 = L_2 = \frac{V_o(1-D)^2 T_s}{2I_o} \tag{3.4}$$

$$C_1 = C_2 = \frac{V_o D T_s}{\Delta V_o R} \tag{3.5}$$

where ΔV_{o} is the oscillation in the output voltage.

The above presented equations serve as the foundation for the parameter estimation process of conventional Ćuk converter. Further, the ripple in input current and output current is expressed as in (3.6) and (3.7).

$$\Delta I_i = \frac{V_i D T_s}{2L_1} \tag{3.6}$$

$$\Delta I_o = \frac{V_i D T_s}{2L_2} \tag{3.7}$$

3.2.2 Merits

Ćuk converter has the unique ability to provide continuous current at both the terminals. Also, as alluded earlier, the voltage waveforms across the input and output inductors are identical [13]. This is the key factor that dictates the ability to couple the separate inductors onto a single magnetic core. With the inclusion of another winding, either in the form of an inductor or a transformer, ripple-free behavior can be evidenced in both the input and output terminals when designed accurately [14]. This is because the voltage waveforms across all of the individual magnetic components remained to be proportional to each other.

3.3 Choice of Topology for Photovoltaic Applications

Ćuk converter has been demonstrated to overcome all the drawbacks declared previously in the prior state-of-the-art architectures. There are various modified versions of the standard Ćuk converter that are designed and analyzed theoretically in the past

which comprise coupled inductor topology [15] [16], isolated Ćuk converter with integrated magnetics [17] [18], ZVS-ZCS Active-Clamp Ćuk converter [19] and others. Several studies have concentrated on describing the theory behind accomplishing zero-ripple terminal currents [20], designing integrated magnetics, area-product method versus geometric constant method to aid magnetics design, small-signal modeling and so on. Nonetheless, it is hard to find a suitable, elegant procedure to realize a zero-ripple input current Ćuk converter topology. This is restraining numerous engineers and researchers from attaining the anticipated results by the use of Ćuk converter in crucial applications such as PV interfaces for which it is ideal. This research work addresses the issue by proposing an analytical design approach. The circuit diagram of a coupled inductor Ćuk converter is as shown in Fig. 3.3.

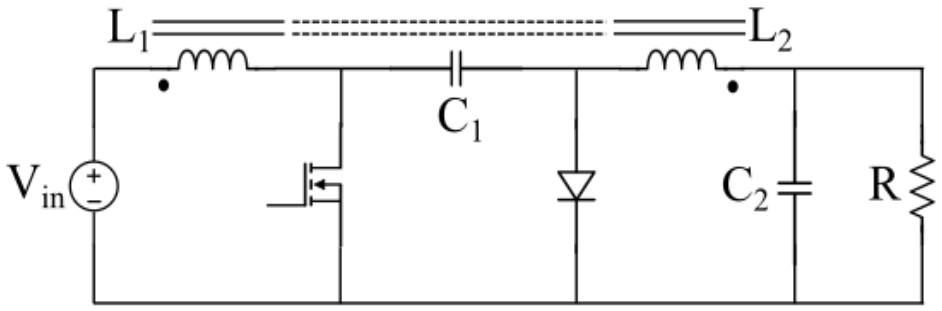

Figure 3.3: Coupled inductor Ćuk converter

3.4 Design Methodology

The circuit analysis can be carried out based on the principle of duality. Two networks are considered to be duals of each other if the loop equations of one network are in the same form as the node equations for the other. Thus, duality can be used in the process of obtaining the circuit model from its equivalent model (reluctance model in this case).

3.4.1 Electrical Circuit Analysis

As depicted for Ćuk converter, comparable investigation needs to be realized for coupled inductor Ćuk converter as well [15]. Because of the existence of coupled inductor and the related magnetics, the analysis and use of Kirchoff's laws is not as simple as in the case of conventional Ćuk converter. In order to proceed with the analysis, let us examine the circuit shown in Fig. 3.3.

When the switch is conducting, the following equations can be obtained:

$$V_i - N_1 \frac{d\phi_1}{dt} = 0 \tag{3.8}$$

$$V_{C_1} - N_2 \frac{d\phi_2}{dt} - V_{C_o} = 0 \tag{3.9}$$

$$-V_o + V_{C_o} = 0 \tag{3.10}$$

The voltage across the inductors in the above equations are based on Faraday's law of induction which relates flux with voltage and is given by (3.11).

$$V = N \frac{d\phi}{dt} \tag{3.11}$$

When the diode is in the on state, the following equations can be written for the circuit in Fig. 3.3:

$$V_i - N_1 \frac{d\phi_1}{dt} - V_{C_1} = 0 \tag{3.12}$$

$$-N_2 \frac{d\phi_2}{dt} - V_{C_o} = 0 \tag{3.13}$$

$$-V_o + V_{C_o} = 0 \tag{3.14}$$

In addition to the electrical analysis, the magnetic equivalent circuit representation of the coupled inductor needs to be scrutinized. To accomplish the same, either reluctance model or gyrator-capacitor model can be utilized. The reason for doing this is to be able to substitute the obtained flux conditions in (3.8) - (3.10) and (3.12) - (3.14) and thus summarize the design conditions for achieving zero-ripple terminal currents.

3.4.2 Equivalent Modeling

The dashed line between the inductors in Fig. 3.3 indicates that they form a coupled inductor. As alluded before, when two inductors are wound on the same magnetic core, a coupled inductor is formed and is similar to a transformer. It is critical to observe that the magnetomotive forces (MMFs) of the two windings are additive for a coupled inductor, which is not true in the case of a transformer. Therefore, a coupled inductor can be expressed using its equivalent reluctance model as in Fig. 3.4.

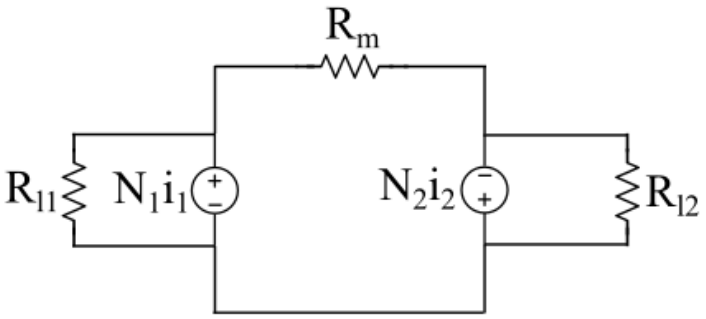

Figure 3.4: Equivalent reluctance model

Reluctance model is implemented by inspecting the physical geometry and the winding locations of an actual magnetic assembly. Magnetic core legs and gaps are modeled as resistors with the resistance equal to their corresponding reluctance while

the windings are replaced by voltage sources [21]. Coupling is the cause behind going with a reluctance model rather than the usual electrical model analysis.

The other popular modeling technique is the gyrator-capacitor model. In this method, core legs and gaps are modeled by capacitors with capacitance equal to their corresponding permeance value. Both the modeling techniques should lead to a similar set of conditions in terms of realizing zero-ripple currents and parameter estimation. The reluctance model is a traditional modeling technique and is being used for years. However, gyrator-capacitor model is a more straight-forward approach as the representation is closer to the geometrical structure of the component and more intuitive. In this work, the analysis is based on the equivalent reluctance model shown in Fig. 3.4.

3.4.3 Magnetic Circuit Analysis

Magnetic analysis can be accomplished by writing the node equations for the equivalent model shown in Fig. 3.4. The following equations can be obtained:

$$\phi_1 - \phi_{l_1} - \phi_m = 0 \tag{3.15}$$

$$-\phi_2 + \phi_{l_2} + \phi_m = 0 \tag{3.16}$$

$$N_1 i_1 + R_{l_1}\phi_{l_1} = 0 \tag{3.17}$$

$$N_1 i_1 + N_2 i_2 - R_m \phi_m = 0 \tag{3.18}$$

$$N_2 i_2 + R_{l_2}\phi_{l_2} = 0 \tag{3.19}$$

where reluctance is represented as R.

Differentiating flux, ϕ terms in (3.15) - (3.19) and re-arranging, we can get the following equations, which can be used in (3.8) - (3.10) and (3.12) - (3.14) to attain the parameter values.

$$\frac{d\phi_{l_1}}{dt} = \frac{N_1}{R_{l_1}}\frac{di_1}{dt} \tag{3.20}$$

$$\frac{d\phi_{l_2}}{dt} = \frac{N_2}{R_{l_2}}\frac{di_2}{dt} \tag{3.21}$$

$$\frac{d\phi_m}{dt} = \frac{N_1}{R_m}\frac{di_1}{dt} + \frac{N_2}{R_m}\frac{di_2}{dt} \tag{3.22}$$

$$\frac{d\phi_1}{dt} = \frac{N_1}{R_{l_1}}\frac{di_1}{dt} + \frac{N_1}{R_m}\frac{di_1}{dt} + \frac{N_2}{R_m}\frac{di_2}{dt} \tag{3.23}$$

$$\frac{d\phi_2}{dt} = \frac{N_2}{R_{l_2}}\frac{di_2}{dt} + \frac{N_1}{R_m}\frac{di_1}{dt} + \frac{N_2}{R_m}\frac{di_2}{dt} \tag{3.24}$$

It is known that the ripple-free property is independent of the current and voltage levels. The presented equations can lead to estimation of parameters based on ripple-free input or output current specifications.

3.4.4 Zero-ripple Currents

In order to achieve ripple free input current, it should be a constant value and thus, its derivative should be zero. This condition yields:

$$\frac{di_1}{dt} = 0 \tag{3.25}$$

This directly translates to:

$$L_{11} \neq L_M; L_{22} = L_M \tag{3.26}$$

In terms of coupling coefficient, (3.26) yields:

$$k = \frac{L_M}{\sqrt{L_{11}L_{22}}} = \frac{L_{22}}{\sqrt{L_{11}L_{22}}} = \sqrt{\frac{L_{22}}{L_{11}}} = \frac{1}{n} \tag{3.27}$$

where n is called the effective turns ratio. This value is almost equal to the actual turns ratio.

Using (3.25) in the previously obtained state equations, we obtain the condition for zero-ripple input current as:

$$\frac{N_1}{N_2} = 1 + \frac{R_m}{R_{l_2}} \tag{3.28}$$

On the same lines, to obtain zero-ripple output current, we have the following conditions:

$$\frac{di_2}{dt} = 0 \tag{3.29}$$

$$L_{11} = L_M; L_{22} \neq L_M \tag{3.30}$$

$$\frac{N_1}{N_2} = \frac{R_{l_1}}{R_{l_1} + R_m} \tag{3.31}$$

Also, based on (3.6) and (3.7), the ripple in input and output currents for coupled inductor Ćuk converter can be represented as below:

$$\Delta I_i = \frac{(L_2 - M)V_i D T_s}{L_1 L_2 - M^2} \tag{3.32}$$

$$\Delta I_o = \frac{(L_1 - M)V_i D T_s}{L_1 L_2 - M^2} \tag{3.33}$$

where M is the mutual inductance.

The obtained reluctance values can be translated to equivalent inductance values using (3.34).

$$L = \frac{N^2}{R} \tag{3.34}$$

3.4.5 Magnetics Design

The zero-ripple condition obtained demonstrates that the leakage inductance of the winding which is bearing the ripple must be controlled appropriately. In this case, it is the output winding. In order to realize a low value of residual ripple and low sensitivity, at least one winding must have relatively high leakage [10].

In order to achieve a relatively high value of leakage inductance that is well controlled, additional leakage inductor can be used with the coupled inductor. This is simple and straightforward but defeats the whole idea of reducing and integrating the magnetic components to achieve better performance.

The other way to achieve relatively high leakage on one of the windings is by building an additional magnetic branch for the leakage flux path in the existing coupled inductor. In the scenario where there are no other leakages in such a structure, the reluctance model for zero input current ripple is as in Fig. 3.5.

Consider the cross sections, S of the outer legs to be the same. This implies:

$$R_x = \frac{x}{\mu_o S} \tag{3.35}$$

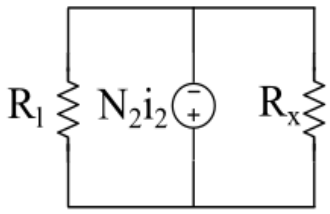

Figure 3.5: Reluctance model for zero ripple in N_1

$$R_l = \frac{l_g}{\mu_o S} \tag{3.36}$$

where l_g is the air gap of the leakage flux path.

The existence of the air gap makes the flux versus Ampere-turn characteristic more linear and is required to prevent the core from saturating. From (3.35) and (3.36), zero ripple condition can be derived as:

$$\frac{x}{l_g} = \frac{N_1}{N_2} - 1 \tag{3.37}$$

When the two air gaps are same $(x = l_g)$, (3.37) yields:

$$N_1 = 2N_2 \tag{3.38}$$

Another possibility of achieving zero ripple input current without even adding an additional magnetic path is by using the leakages of the winding only. However, this enforces stricter design measures specifically on the leakage parameter l, which needs to be appropriately represented and assessed for a wide variety of cores in terms of varied shapes and geometries ahead of time. It is represented as:

$$l = R_l \mu_o S \tag{3.39}$$

where μ_o is the permeability.

Chapter 4

Converter Implementation and Validation

4.1 Simulation Results

The sample design of the proposed coupled inductor Ćuk converter is accomplished for the specifications in table 4.1.

Table 4.1: Input Parameters

Parameters	Values
Input Voltage (V)	30
Output Voltage (V)	300
Output Power (W)	250
Switching Frequency (kHz)	100
Zero-ripple condition	Input current

The estimation of parameters for the necessary components based on the given requirements is executed based on the method as outlined in Fig. 4.10. MATLAB scripts and Analysis-Led Design (ALD) tool realized using Microsoft Excel are used in the process along with verification using manual calculations. The key component values thus gathered are shown in table 4.2.

The reluctance values obtained based on design is used in ANSYS to model the

Table 4.2: Component Values

Parameters	Values
Magnetizing Turns N_1	28
Magnetizing Turns N_2	54
Input Capacitor, C_1 (μF)	55
Coupling Capacitor, C_2 (nF)	90
Resistance, R (Ω)	150

overall converter. In Fig. 4.1, modeling is accomplished with magnetizing reluctance represented in orange. Another possible circuit realization is as modeled in Fig. 4.2 where the complete reluctance model with leakage reluctances are modeled along with the electrical components of the converter circuit. The simulation behavior validates the theoretical analysis and equivalent modeling based on reluctance model.

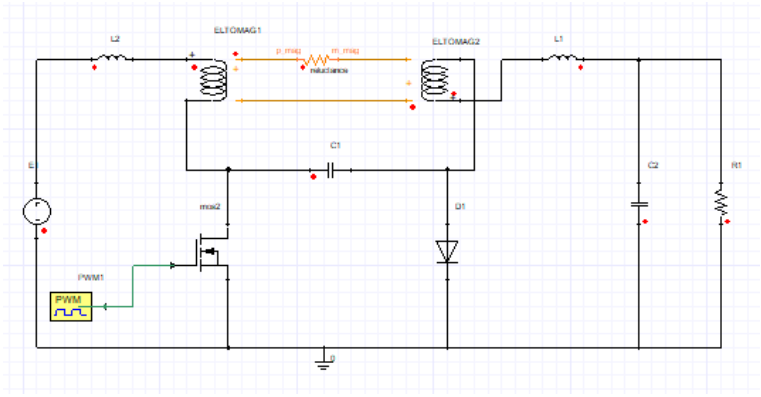

Figure 4.1: Simulation model of coupled inductor Ćuk converter in ANSYS

The procured results are incorporated in the PLECS simulation. The circuit of the coupled inductor Ćuk converter realized using the PLECS platform is as shown in Fig. 4.3.

Equivalently, the conventional Ćuk converter topology is also simulated using the PLECS software. The input current waveforms obtained for both the topologies are shown in Fig. 4.4. The zoomed versions of the input current waveforms observed for both the topologies are shown in Fig. 4.5. It is evident that the ripple in the input current is observed to be 13.79% for the conventional Ćuk converter topology. However, the

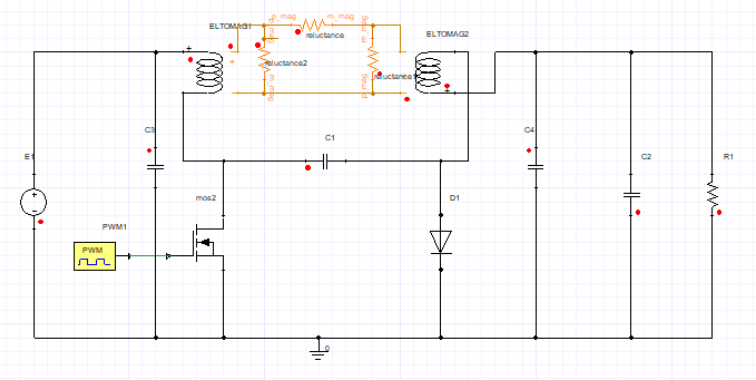

Figure 4.2: Simulation model of coupled inductor Ćuk converter in ANSYS with leakage reluctances

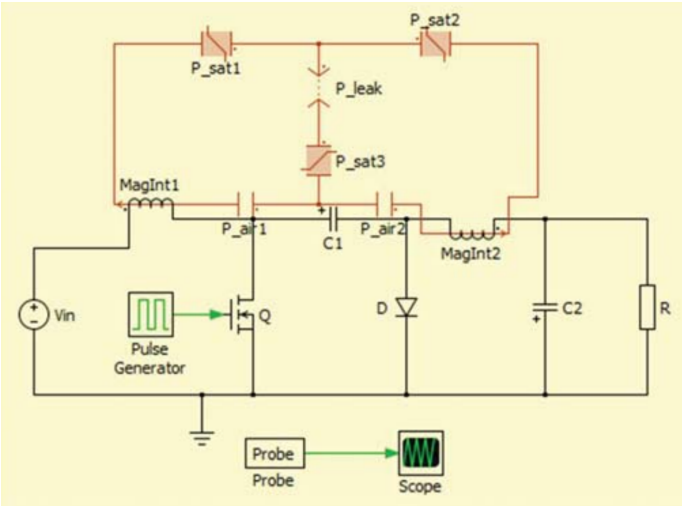

Figure 4.3: Simulation model of coupled inductor Ćuk converter in PLECS

ripple in the input current for coupled inductor Ćuk converter topology is observed to be 2.56%. It is evident that the ripple in the input current can be minimized by the use of coupled inductor. The negligible value of the ripple noticed is likely because of the manner in which the magnetics are simulated and approximations of the values are estimated in order to match the standard magnetic component values.

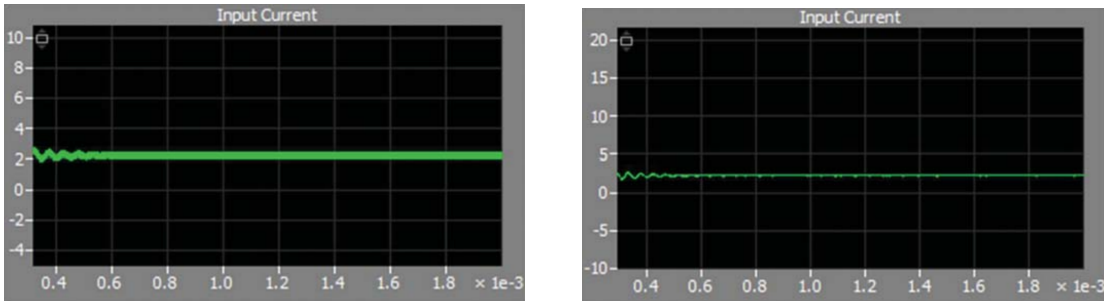

Figure 4.4: Input current characteristics: (a) Ćuk converter, (b) Coupled inductor Ćuk converter

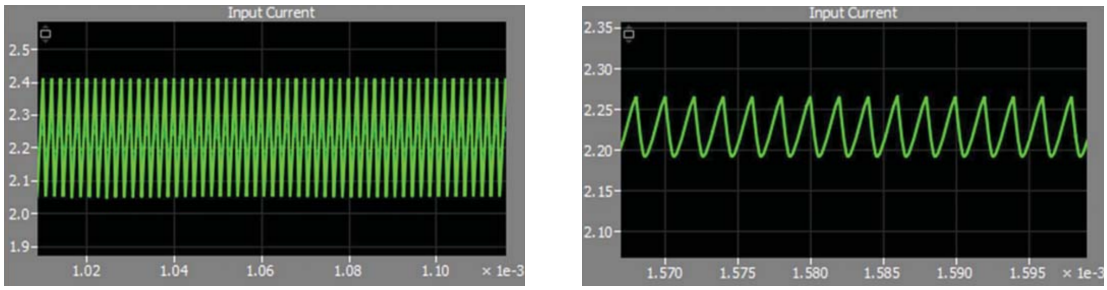

Figure 4.5: Zoomed input current characteristics: (a) Ćuk converter, (b) Coupled inductor Ćuk converter

4.2 Controller Design

The high-level block representation of the system and controller is as shown in Fig. 4.6.

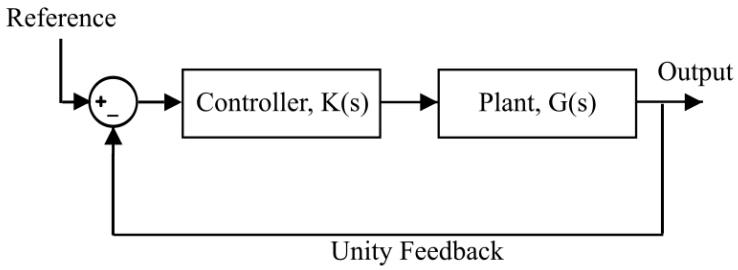

Figure 4.6: Closed-loop control

The idea here is that the error signal, which is the difference between the reference signal and output of the plant is fed to the controller which generates controlled input in order to match the plant output with the reference provided. This is called closed-loop control.

The converter design is focused on obtaining zero input current ripple while having decent performance improvement as compared to the conventional topology. The control method needs to be chosen such that it aids the design requirements. Since input current control is essential, current mode control can be chosen [22]. Here, input inductor current and output capacitor voltage are controlled. Since the current changes faster than the voltage, inner current loop implementation is considered. Outer loop is formed by the output voltage by providing a reference value for the input current based on the value of the output voltage. Also, the controller in a Ćuk converter needs to be able to respond to a negative feedback voltage. This is taken care of during the design process. The block diagram representing the controller design is as shown in Fig. 4.7.

The output voltage error is computed as the difference between the reference output voltage, V_o^{ref} and the output voltage at that time instant. v_o. This error is processed by the voltage controller, G_C^v and produces an instantaneous input current reference, i_i^{ref}. On the same lines, the difference between i_i^{ref} and the input current at that instant, i_i

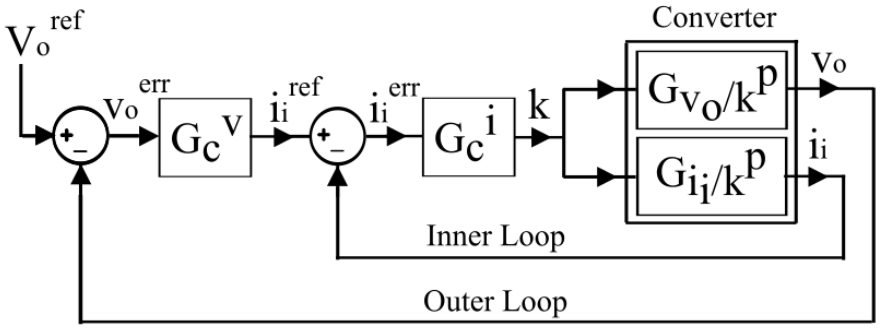

Figure 4.7: Controller block diagram

gives an input current error, i_i^{err}. Then, this error is processed by the current controller, G_C^i and produces a duty factor, k. This duty factor is applied to the converter and the converter produces i_i and V_o according to the input current to duty factor transfer function, $G^p_{\frac{i_i}{k}}$ and output voltage to duty factor transfer function, $G^p_{\frac{v_o}{k}}$. Further, v_o and i_i are taken as feedback and this control cycle is repeated continuously for a few iterations till the error is zero. As discussed, the faster variable, i_i is placed in the inner loop. Even though there are two cascaded loops, it is important to note that there is only one manipulated variable and that is, the duty factor, k.

The transfer function is given by:

$$G^p_{\frac{v_o}{i_i}}(s) = \frac{v_o(s)}{i_i(s)} = \frac{\frac{v_o(s)}{k_s(s)}}{\frac{i_i(s)}{k_s(s)}} = \frac{G^p_{\frac{v_o}{k}}(s)}{G^p_{\frac{i_i}{k}}(s)} \tag{4.1}$$

Equation (4.1) yields:

$$v_o(s) = i_i(s)G^p_{\frac{v_o}{i_i}}(s) = kG^p_{\frac{i_i}{k}}(s)\frac{G^p_{\frac{v_o}{k}}(s)}{G^p_{\frac{i_i}{k}}(s)} = kG^p_{\frac{v_o}{k}}(s) \tag{4.2}$$

The plant in this control system has a fourth-order transfer function. The controller design has the typical inner current and outer voltage loops. In such cases, a proportional-integral (PI) controller seems to be the most appropriate choice as it is

easy to implement and achieves satisfactory results. The integral term helps the steady-state error to be maintained at zero. The main constraints that need to be kept in mind during the design of the controller are:

- Closed-loop stability of the system.
- Fast transient response for tracking changes in reference input.
- Zero steady-state error in reference tracking.

The PI controller considered here is of parallel form and is given by:

$$K(s) = k_p + \frac{k_i}{s} \tag{4.3}$$

where k_p is the proportional gain and k_i is the integral gain. For satisfying the previously stated conditions, following constraints are placed on the PI controller design:

- Open Loop Gain Margin $\geq$ 6 dB
- Open Loop Phase Margin $\geq 60^\circ$

Using (4.1) and (4.2), the controller design is carried out using MATLAB. The design parameters obtained from simulation are substituted and the obtained transfer functions are validated by means of step responses. The 'sisotool' is used to perform gain iteration. The Bode plot for the closed-loop transfer function is as shown in Fig. 4.8. Similarly, the results for $G_{OL}^{v}(s)$ is as shown in Fig. 4.9

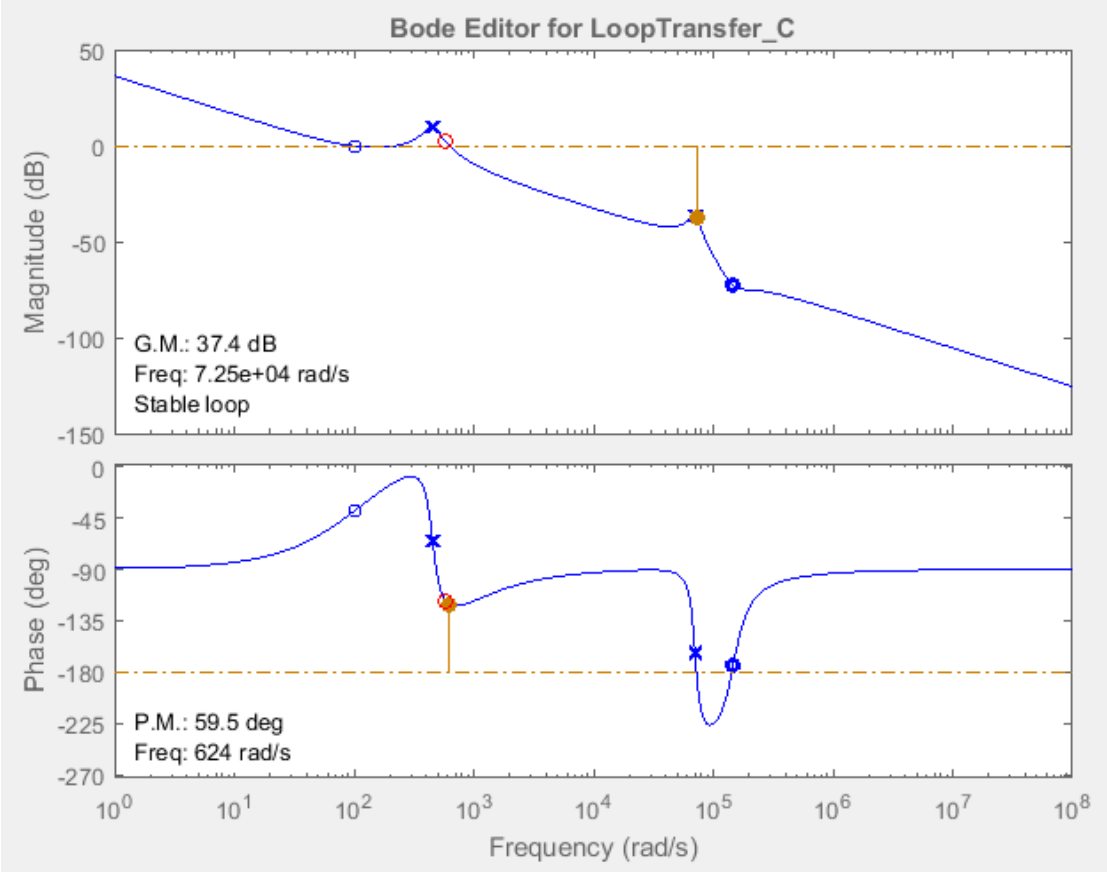

Figure 4.8: Bode plot of closed loop transfer function, current loop $G^i_{CL}(s)$

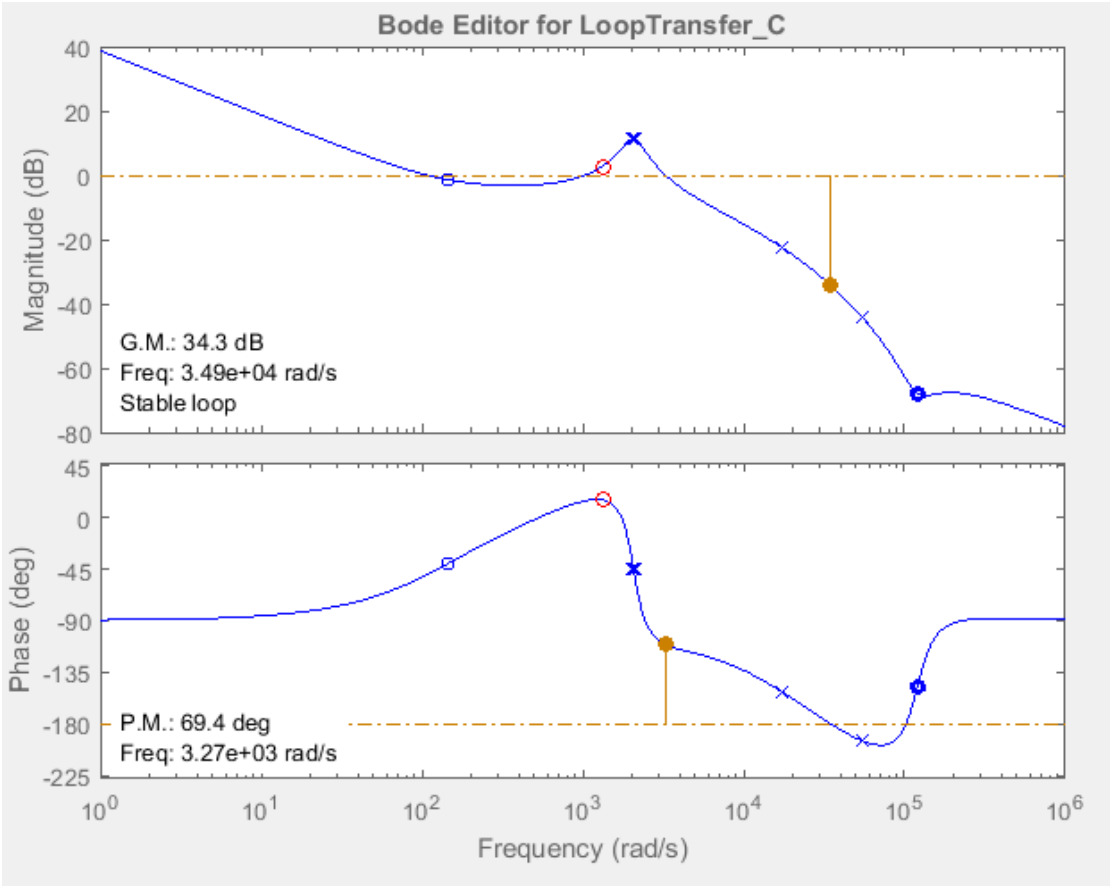

Figure 4.9: Bode plot of closed loop transfer function, voltage loop $G_{CL}^{v}(s)$

4.3 Hardware Setup

The following operating conditions are considered during the design of the coupled inductor Ćuk converter hardware prototype:

- Input voltage range is considered to be 30-40 V considering the PV system to be the DC input source.
- Output voltage is 300 V.
- Converter is designed to supply 250 W for the mentioned voltage ranges.
- Since PV is connected on the input side, it is advisable to have as low ripple as attainable on the input current of the converter. Thus, coupled inductor Ćuk converter with ripple-free input current version is chosen.

The details of the design process is as summarized in Fig. 4.10 and the hardware setup is as shown in Fig. 4.12.

4.3.1 Selection of Components

The use of MOSFET seems to be ideal due to the operating voltage range, currents and switching frequency. It also promises lower losses than its counterpart, IGBT. Based on the calculations of the possible voltage and current stresses on the switch, PCA9517A is chosen.

Schottky diode is chosen due to its low on-state voltage drop and low reverse recovery time. It is typically used for high-frequency operation due to its capability and SiC-based diode is chosen as it is optimized for PFC boost application. Based on the calculations of the possible voltage and current stresses on the diode, C3D02060E by Cree is chosen.

The input coupling capacitor is chosen based on the possible voltage ripple on it due to high-frequency operation. Also, power dissipation is expected to be low to avoid overheating. A capacitor with low ESR is chosen and P123456CT-ND by Panasonic is selected. Aluminum electrolytic type capacitor is chosen due to its high energy density.

The output filter capacitor does not face severe current stress. However, low voltage ripple and low power loss is desirable. Thus, 445-7765-1-ND ceramic capacitor is chosen.

Coupled inductor is chosen such that ripple-free input current is achieved as per the design requirements. Required inductance values, current carrying capability determined based on simulations, appropriate core and coupling specifications are accounted for during the choice. Ferrite core is chosen due to low saturation flux density and low hysteresis loss.

4.3.2 Block Representation

The system hardware for one channel is represented using the block diagram in Fig. 4.11. The gate driver IC is used to generate pulses for the switch in the power converter. The power converter comprises of the circuit implementation using a printed circuit board (PCB), coupled inductor and controller to generate the necessary duty cycle for the circuit operation. The input and output currents of the power converter are measured using current sensors. No onboard power supplies have been used as power sources for the converter or the various ICs. All power supplies are externally connected. Also, the signal and power grounds have been isolated during the design of the PCB.

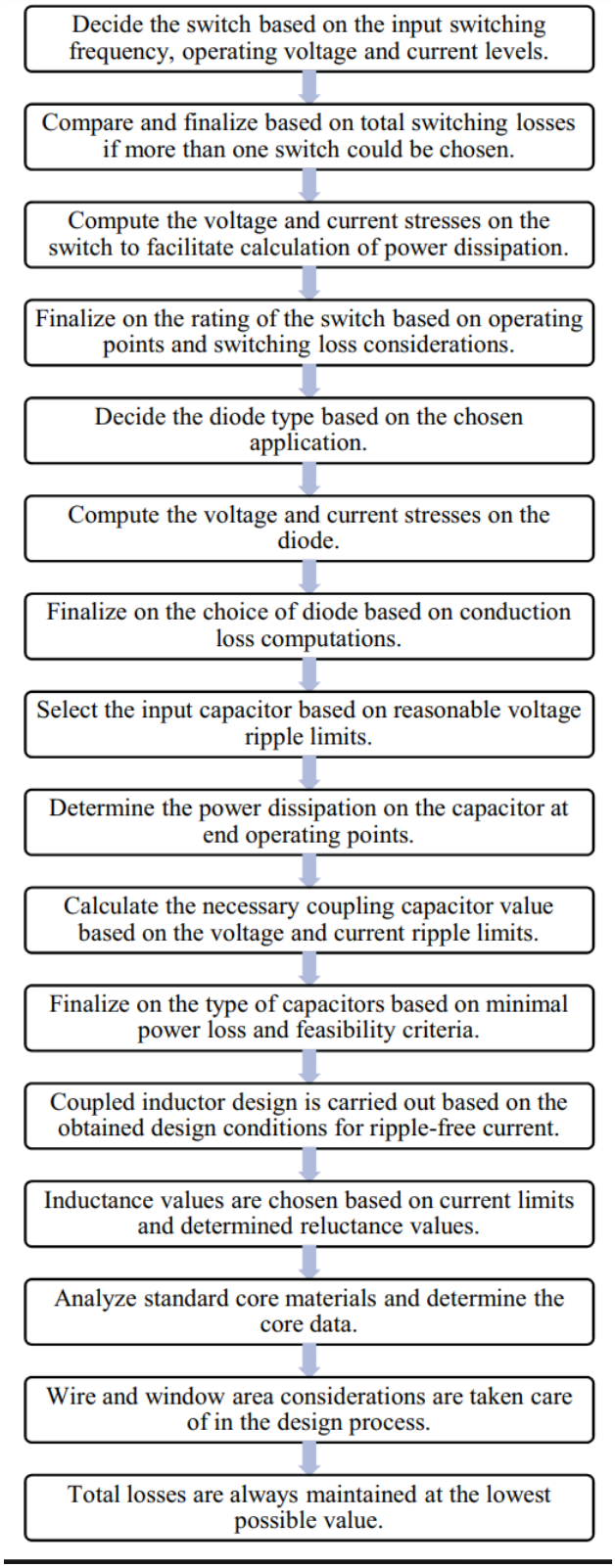

Figure 4.10: Process chart illustrating the design summary of the converter

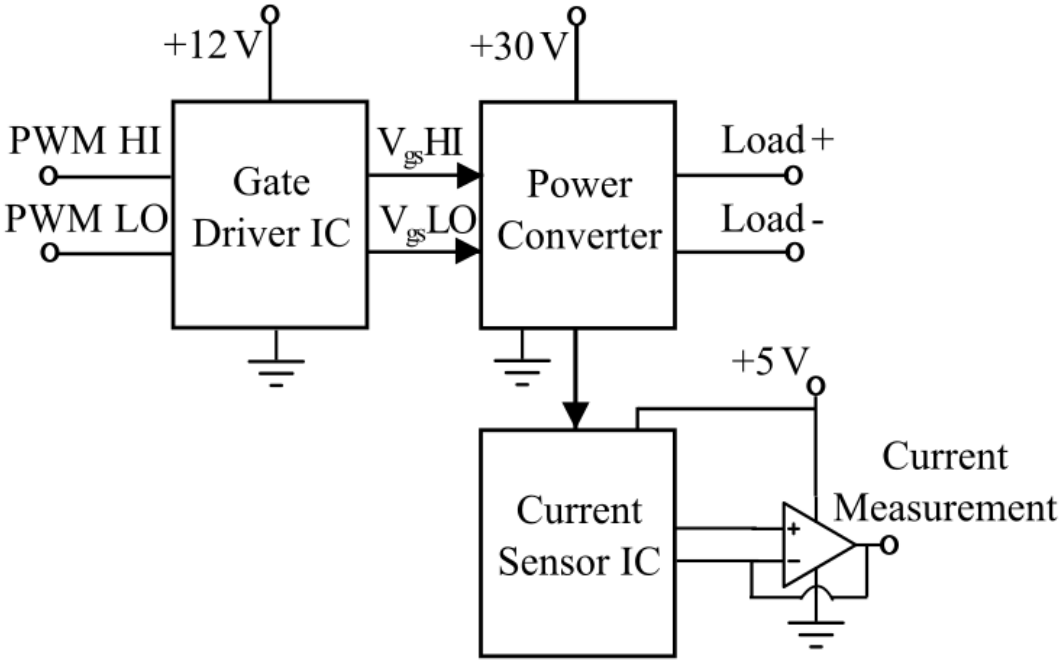

Figure 4.11: System hardware block diagram for a single channel

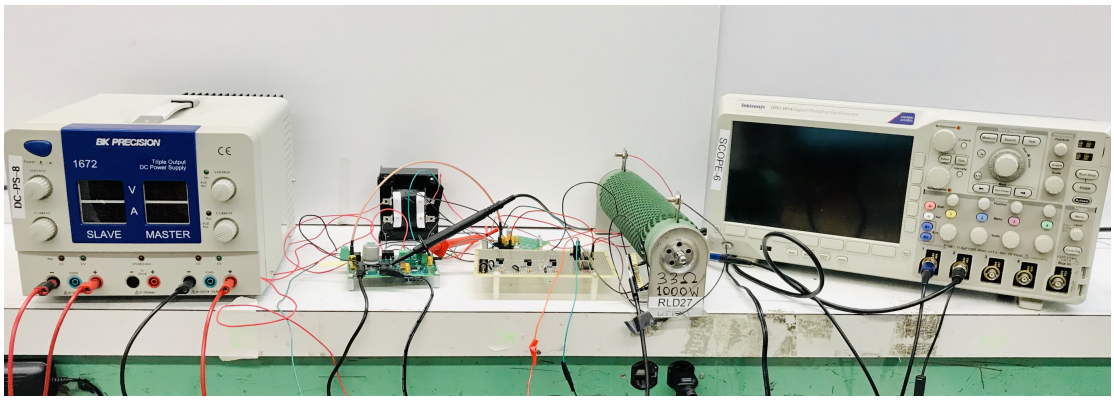

Figure 4.12: Experimental setup

4.4 Experimental Results

The system is validated for closed-circuit operation, expected behavior and input current waveforms are measured. From Fig. 4.13, it is evident that the ripple in the input current is low as per the design and implementation requirements. From Fig. 4.14, the ripple percentage is determined to be about 2.7%.

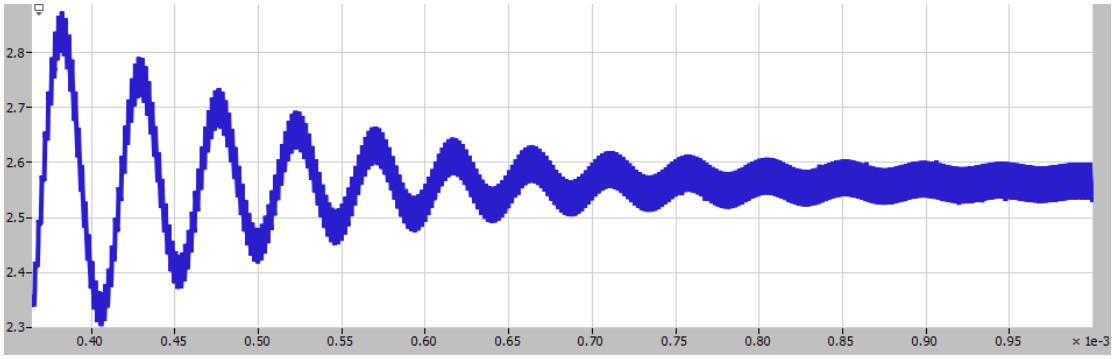

Figure 4.13: Input current waveform

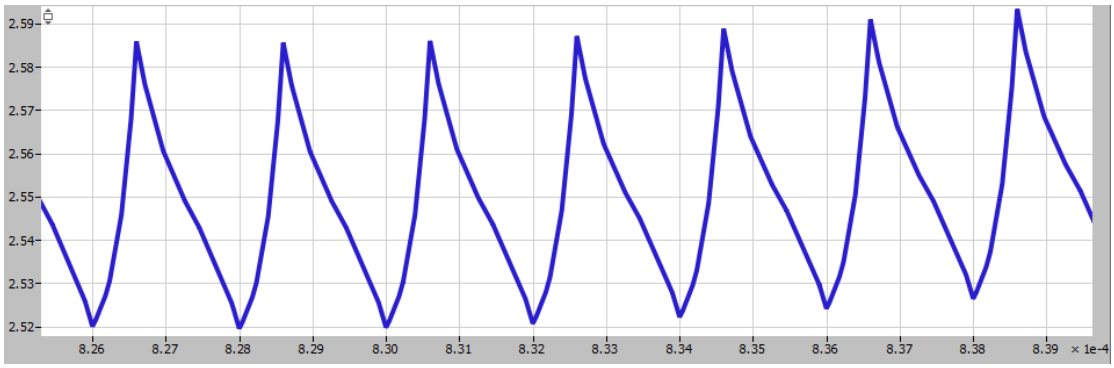

Figure 4.14: Input current waveform - Zoomed

Chapter 5

System Analysis

5.1 Loss Analysis

When two inductors have the same voltage waveforms, they can be integrated into a single structure. This leads to a reduction in usage of the core which in turn leads to compact and lesser weight structure with reduced core loss, no change in copper loss and same energy storage capability. This also enhances the performance due to improved efficiency.

The performance analysis of the converter with coupled inductor is achieved by computing several loss components and by estimating performance parameters for analysis [23]. The power loss in a switch can be divided into two key components namely, conduction and switching losses.

5.1.1 Conduction Loss

The resistive element of the switch leads to power dissipation when current flows through it. This is known as conduction loss and is found to be inversely proportional to the size of the switch. These losses are directly dependent on the duty cycle of the converter as they arise due to parasitic resistances [24]. In simple terms, conduction

loss can be represented as in (5.1).

$$P_{cond} = I_{rms}^2 R_{on} \tag{5.1}$$

where I_{rms} is the rms value of the current and R_{on} is the on-state resistance. In case of a MOSFET employed in a simple converter, the conduction loss is represented as in (5.2).

$$P_{cond} = I_o^2 R_{on} \frac{V_o}{V_{in}} \tag{5.2}$$

where I_o is the output current, R_{on} is the on-state resistance, V_o is the output voltage and V_{in} is the input voltage.

5.1.2 Switching Loss

Switching loss is the other component of power loss. During turn-on and turn-off transitions of the switch, energy is stored and dissipated by the intrinsic capacitor which leads to switching loss. It is proportional to the switching frequency and the value of the parasitic capacitance. Generally, the value of the capacitance is comparable to the physical size of the switch. In simple terms, switching loss can be represented as in (5.3) and (5.4).

$$P_{sw} = V_{in} I_o T_{sw} f_{sw} \tag{5.3}$$

where V_{in} is the input voltage, I_o is the output current, T_{sw} is the switching time and f_{sw} is the switching frequency.

$$P_{sw} = \frac{1}{2} V_{in} I_o (t_r + t_f) f_{sw} \tag{5.4}$$

where V_{in} is the input voltage, I_o is the output current, t_r is rise time and t_f is fall

time.

A rectification or freewheeling diode is often connected in parallel to a MOSFET. This is done in order to ensure current continuity. During continuous conduction mode (CCM) of the converter, turn-on loss is the key reason for lower efficiency which is mostly due to the recovery parameters of the diode. Turn-off loss could be due to the diode working in rectifying mode or the power loss due to the reverse recovery current of an ultra-fast diode. Apart from the turn-on and turn-off losses, forced commutation of the MOSFET's body diode is a prominent source of switching loss in high-voltage DC-DC converters.

5.1.3 Inductor Loss

Inductor loss is a component of conduction loss that occurs when current flows through the inductor. It can be represented as in (5.5).

$$P_l = I_{rms-l}^2 R_{dcr} \tag{5.5}$$

where I_{rms-l} is the rms value of inductor current represented as in (5.6) and R_{dcr} is the DC resistance of the inductor.

$$I_{rms-l}^2 = I_o^2 + \frac{\Delta I^2}{12} \tag{5.6}$$

where I_o is the output current and ΔI is the ripple current. The ripple current is usually around 30% of the output current in typical cases. Thus, it can be represented as in (5.7).

$$I_{rms-l} = 1.0037 I_o \tag{5.7}$$

Note that since the ripple current contributes to approximately 0.37% of I_{rms-l}, it

is neglected in some of the calculations and I_o is used directly in (5.5) for conventional converters.

The inductor loss is typically a combination of core loss and winding loss.

Core Loss

Core loss occurs in a magnetic core due to alternating magnetization. It comprises of hysteresis and eddy current losses [25]. Total core loss can be expressed as in (5.8).

$$P_{l-core} = V_e P_{\frac{C}{V}} \tag{5.8}$$

where V_e is the effective volume of the core and $P_{\frac{C}{V}}$ is the core loss per unit volume.

Winding Loss

Winding or copper loss is the heat produced by currents in the conductors of transformer windings or other wound components. It justifies the skin and proximity effects. Total winding loss can be defined as in (5.9).

$$P_{l-wndg} = I_l^2 R_{dc} + I_{l-rms}^2 R_{dc} \tag{5.9}$$

where I_l is the average value of inductor current, I_{l-rms} is the AC rms current and R_{dc} is the dc value of the winding resistance.

5.1.4 Other Losses

In addition to the components of the power loss that are previously elaborated, there are other prominent losses that influence the overall performance of the system.

Gate charge loss is the power dissipated due to the charging and discharging of the gate of the switch. It can be represented as in 5.10.

$$P_{gc} = 2V_{driver}Q_g f_{sw} \tag{5.10}$$

where V_{driver} is the gate drive voltage and Q_g is the total gate charge.

Diode power loss is the loss that occurs when diode is conducting and is expressed as in 5.11.

$$P_{diode} = V_f I_d \tag{5.11}$$

where V_f is the diode forward voltage drop and I_d is the average current that passes through the diode in one switching cycle.

Filter capacitor loss can be obtained as in (5.12).

$$P_c = I_{rms-c}^2 ESR_c \tag{5.12}$$

where I_{rms-c} is the rms value of the current through capacitor and ESR_c is the equivalent series resistance of the capacitor.

5.1.5 Performance Analysis

With the aid of all the equations obtained in the previous subsections, loss analysis is accomplished for the basic Ćuk converter and coupled inductor Ćuk converter topologies using MATLAB scripts and Simulink blocks. The high-level simulation model of the same is as shown in Fig. 5.1. The results obtained are compared and it is evident that the losses have reduced considerably in the coupled inductor Ćuk converter topology mostly due to the integration of magnetic components and careful consideration of design aspects. The obtained values of various losses are compared and contrasted in Fig. 5.2. Also, the resulting performance metrics are presented in Fig. 5.3.

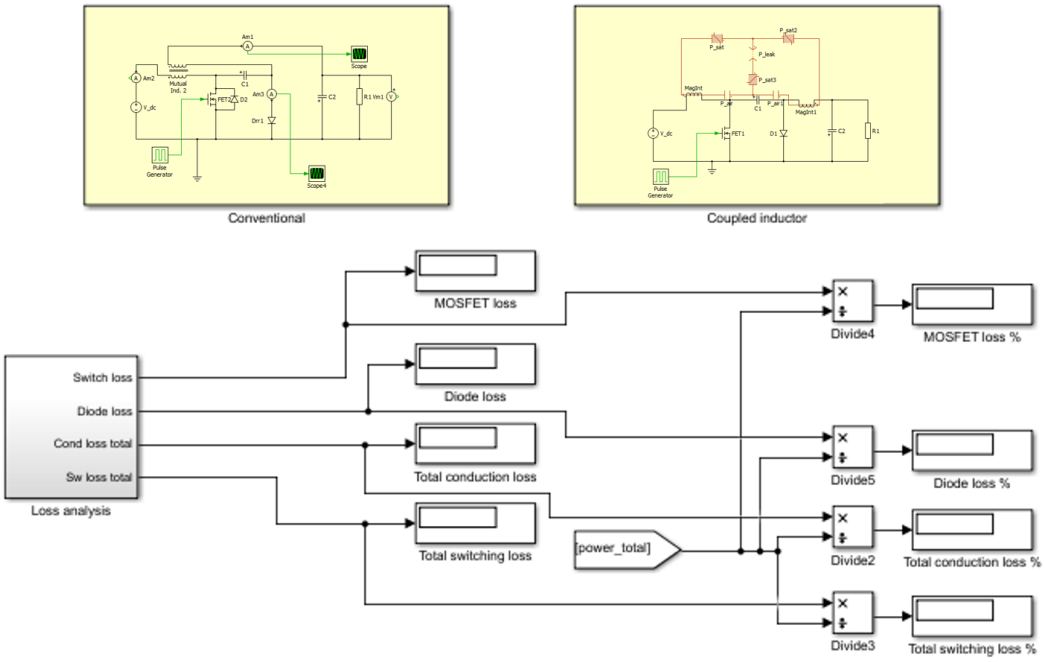

Figure 5.1: Loss Analysis Simulation

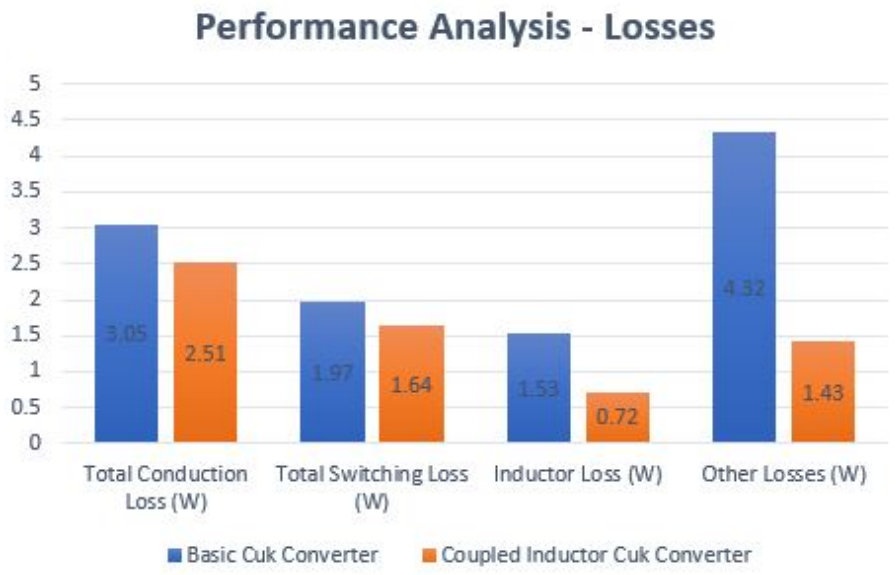

Figure 5.2: Performance Analysis - Losses

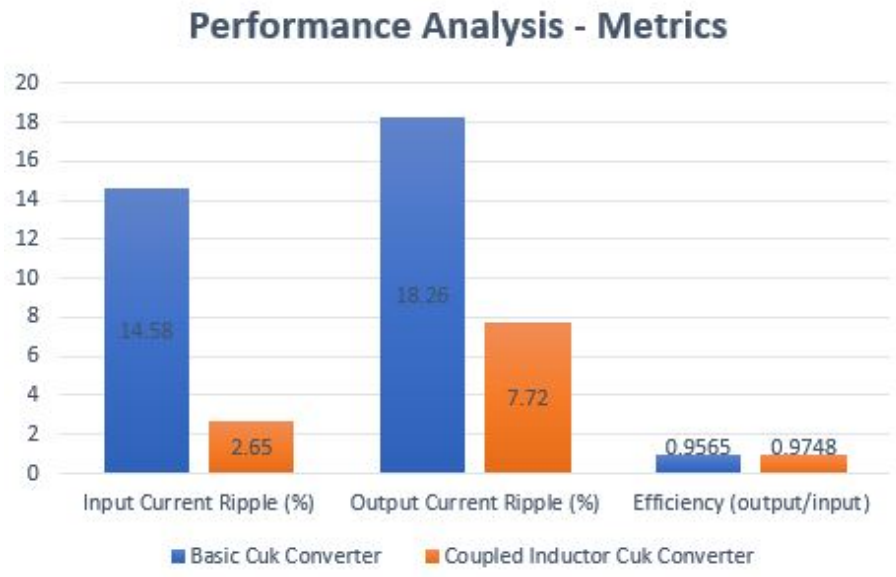

Figure 5.3: Performance Analysis - Metrics

5.2 IEEE 1547 Standards

IEEE 1547 (Standard for Interconnecting Distributed Resources with Electric Power Systems) is a standard of the Institute of Electrical and Electronics Engineers (IEEE) that aims at providing a set of criteria and requirements for the interconnection of distributed energy resources (DERs) into the power grid [26]. It helps foster a systematic standard for the interconnection of distributed resources with Electric Power Systems (EPSs) and requirements applicable to the performance, operation, testing, safety, and maintenance of the interconnection. This, along with UL 1741 standards for inverters and converters govern the overall system design of photovoltaics interconnected with grid or storage using converters and inverters.

IEEE 1547 specifically covers the technical specifications and requirements for the power interfaces between the DERs and EPS, along with its validation. The system designed is validated for the major guidelines set by IEEE 1547 including conditions around voltage regulation, grounding and monitoring, and the design is such that it passes all the necessary requirements. The simulation model is built using the MATLAB/Simulink platform and the high-level test system is as depicted in Fig. 5.4. It comprises of the solar panel, proposed converter interfaced with the inverter and integrated with the grid. Also, UL 1741 standards around the interconnection of equipments are reviewed for system rating and protection aspects.

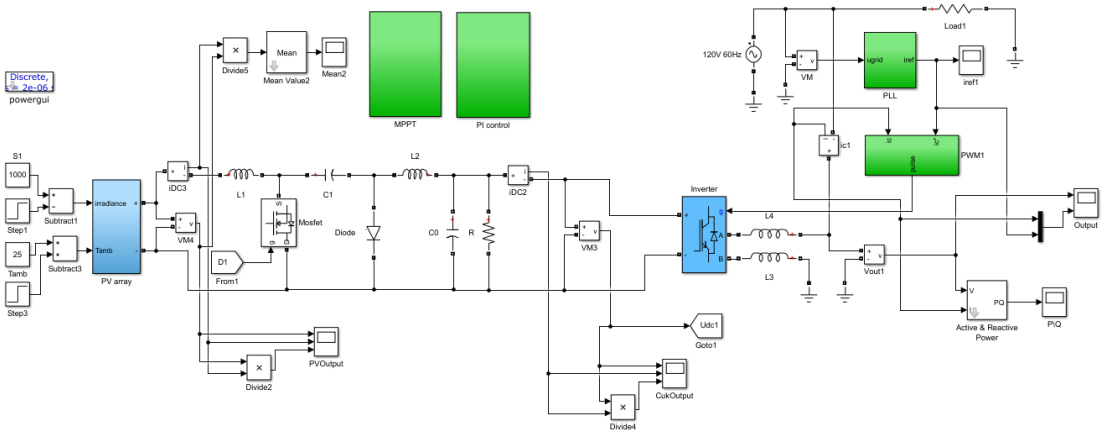

Figure 5.4: Simulation model to validate the IEEE 1547 Standards

Chapter 6

Conclusion and Future Work

6.1 Conclusion

This thesis presents a comprehensive explanation of the need for DC-DC converters and the priority for achieving ripple free input current for photovoltaic applications. The conventional Ćuk converter is introduced and the need for integrated magnetics is emphasized. Zero-ripple conditions for the coupled inductor Ćuk converter topology are obtained based on basic circuit analysis using the equivalent reluctance modeling method. The process chart illustrating the key steps appropriated during the parameter estimation procedure are summarized. The highlights of the magnetic design aspects are reiterated. The results contrasting the coupled inductor Ćuk converter topology with the basic Ćuk converter topology are pointed out. With reference to the ripple content noticed in the input current, it is clear that the use of coupled inductor is advantageous over the conventional topology and the design conditions obtained by means of circuit analysis are critical in the process of estimating the component values. The novelty of the research in terms of basic circuit analysis and step-by-step parameter estimation approach are asserted. A PI controller is designed to validate the closed-loop system behavior and the resulting pole-zero and Bode plots are presented. Laboratory prototype for the designed converter is implemented and experimental results are presented. They

are found to be in consensus with the theoretical analysis and simulation results. Also, loss analysis and performance analysis are carried out at the system level and the results obtained are presented.

6.2 Future Work

There are several future research opportunities, especially related to the design of magnetics.

The study can be extrapolated to other crucial topologies with magnetics involved in the design process and there by, a parameter estimation procedure can be summarized. Also, a tool can be built to accomplish the same. This enables the ease of design of converters for PV integration in general and specifically with integrated magnetics.

Ćuk converter with integrated magnetics, that is, topology with isolation can be investigated in the similar lines. However, special design aspects with respect to magnetic structure needs to be realized in this case.

Equivalent modeling using gyrator capacitor technique can be investigated to provide a more physical design approach. Also, other control techniques can be investigated.

References

[1] W. Li and X. He. “Review of Nonisolated High-Step-Up DC/DC Converters in Photovoltaic Grid-Connected Applications”. In: *IEEE Transactions on Industrial Electronics* 58.4 (Apr. 2011), pp. 1239–1250. ISSN: 1557-9948. DOI: 10.1109/TIE.2010.2049715.

[2] S. Cuk and R. D. Middlebrook. “Advances in Switched-Mode Power Conversion Part I”. In: *IEEE Transactions on Industrial Electronics* IE-30.1 (Feb. 1983), pp. 10–19. ISSN: 1557-9948. DOI: 10.1109/TIE.1983.356697.

[3] P. R. K. Chetty. “Modelling and Analysis of Cuk Converter Using Current Injected Equivalent Circuit Approach”. In: *IEEE Transactions on Industrial Electronics* IE-30.1 (Feb. 1983), pp. 56–59. ISSN: 1557-9948. DOI: 10.1109/TIE.1983.356705.

[4] Marian K Kazimierczuk. *Pulse-width modulated DC-DC power converters*. John Wiley & Sons, 2015.

[5] H. Krishnaswami and N. Mohan. “Three-Port Series-Resonant DC–DC Converter to Interface Renewable Energy Sources With Bidirectional Load and Energy Storage Ports”. In: *IEEE Transactions on Power Electronics* 24.10 (Oct. 2009), pp. 2289–2297. ISSN: 1941-0107. DOI: 10.1109/TPEL.2009.2022756.

[6] Robert W Erickson and Dragan Maksimovic. *Fundamentals of power electronics*. Springer Science & Business Media, 2007.

[7] M. S. Agamy et al. “Dc-dc converter topology assessment for large scale distributed photovoltaic plant architectures”. In: *2011 IEEE Energy Conversion Congress and Exposition*. Sept. 2011, pp. 764–769. DOI: 10.1109/ECCE.2011.6063847.

[8] J. P. Lee et al. “High efficient interleaved input-series-output-parallel-connected DC/DC converter for photovoltaic power conditioning system”. In: *2009 IEEE Energy Conversion Congress and Exposition*. Sept. 2009, pp. 327–329. DOI: 10.1109/ECCE.2009.5316517.

[9] R. L. Steigerwald. “A comparison of half-bridge resonant converter topologies”. In: *IEEE Transactions on Power Electronics* 3.2 (Apr. 1988), pp. 174–182. ISSN: 1941-0107. DOI: 10.1109/63.4347.

[10] Zhe Zhang. “Coupled-inductor magnetics in power electronics”. PhD thesis. California Institute of Technology, 1987.

[11] Ned Mohan, Tore M Undeland, and William P Robbins. *Power electronics*. Wiley New York, 2011.

[12] I. Colak et al. “Design of a parameter determination system for non-isolated converter topologies”. In: *International Aegean Conference on Electrical Machines and Power Electronics and Electromotion, Joint Conference*. Sept. 2011, pp. 240–243. DOI: 10.1109/ACEMP.2011.6490603.

[13] Muhammad H Rashid. *Power electronics handbook: devices, circuits and applications*. Elsevier, 2010.

[14] S. Cuk. “A new zero-ripple switching DC-to-DC converter and integrated magnetics”. In: *IEEE Transactions on Magnetics* 19.2 (Mar. 1983), pp. 57–75. ISSN: 1941-0069. DOI: 10.1109/TMAG.1983.1062238.

[15] A. Ramanath, A. Kshirsagar, and N. Mohan. “Analysis of Current Ripple in Ćuk Converter Topologies - A Novel Approach”. In: *2018 IEEE International Con-*

ference on Power Electronics, Drives and Energy Systems (PEDES). Dec. 2018, pp. 1–6. DOI: 10.1109/PEDES.2018.8707913.

[16] J. W. Kolar et al. “Novel aspects of an application of ’zero’-ripple techniques to basic converter topologies”. In: *PESC97. Record 28th Annual IEEE Power Electronics Specialists Conference. Formerly Power Conditioning Specialists Conference 1970-71. Power Processing and Electronic Specialists Conference 1972*. Vol. 1. June 1997, 796–803 vol.1. DOI: 10.1109/PESC.1997.616810.

[17] A. Ramanath et al. “Equivalent Modeling, Design and Analysis of Integrated Magnetics Ćuk Converter”. In: *2019 North American Power Symposium (NAPS)*. Oct. 2019, pp. 1–6. DOI: 10.1109/NAPS46351.2019.9000277.

[18] A. A. Aboulnaga and A. Emadi. “Performance evaluation of the isolated bidirectional Cuk converter with integrated magnetics”. In: *2004 IEEE 35th Annual Power Electronics Specialists Conference (IEEE Cat. No.04CH37551)*. Vol. 2. June 2004, 1557–1562 Vol.2. DOI: 10.1109/PESC.2004.1355657.

[19] S. Biswas and N. Mohan. “A hybrid soft-switching integrated magnetic Ćuk converter for photovoltaic applications”. In: *2013 7th IEEE GCC Conference and Exhibition (GCC)*. Nov. 2013, pp. 199–203. DOI: 10.1109/IEEEGCC.2013.6705775.

[20] K. C. Daly. “Ripple determination for switch-mode DC/DC converters”. In: *IEE Proceedings G - Electronic Circuits and Systems* 129.5 (Oct. 1982), pp. 229–234. ISSN: 0143-7089. DOI: 10.1049/ip-g-1.1982.0040.

[21] Liang Yan and B. Lehman. “A capacitor modeling method for integrated magnetic components in DC/DC converters”. In: *IEEE Transactions on Power Electronics* 20.5 (Sept. 2005), pp. 987–996. ISSN: 1941-0107. DOI: 10.1109/TPEL.2005.854018.

[22] S. Chattopadhyay and S. Das. “A Digital Current-Mode Control Technique for DC–DC Converters”. In: *IEEE Transactions on Power Electronics* 21.6 (Nov. 2006), pp. 1718–1726. ISSN: 1941-0107. DOI: 10.1109/TPEL.2006.882929.

[23] A. Ramanath and N. Mohan. “Performance Analysis of GaN-based Converter with Integrated Magnetics”. In: *2020 IEEE International Conference on Power Electronics, Smart Grid and Renewable Energy (PESGRE2020)*. 2020, pp. 1–5.

[24] Narendra Mehta. “GaN FET module performance advantage over silicon”. In: *Application Note, Texas Instruments* (2015).

[25] M. Wasekura, C. Wang, and R. D. Lorenz. “A transient core loss analysis of multiple-gap inductor designed for the 2010 Prius”. In: *2014 IEEE Energy Conversion Congress and Exposition (ECCE)*. Sept. 2014, pp. 2177–2181. DOI: 10.1109/ECCE.2014.6953692.

[26] David J Narang and Michael Ingram. *Highlights of IEEE Standard 1547-2018*. Tech. rep. National Renewable Energy Lab.(NREL), Golden, CO (United States), 2019.

Appendix A

Principle of Duality

The principle of duality can be explained using an example as shown in Fig. A.1. In this, (a) Determining the dual circuit structure, (b) The dual circuit, (c) Scaling the permeances by N^2, (d) The circuit model and (e) Scaling by an ideal transformer to match the input and output voltages and currents.

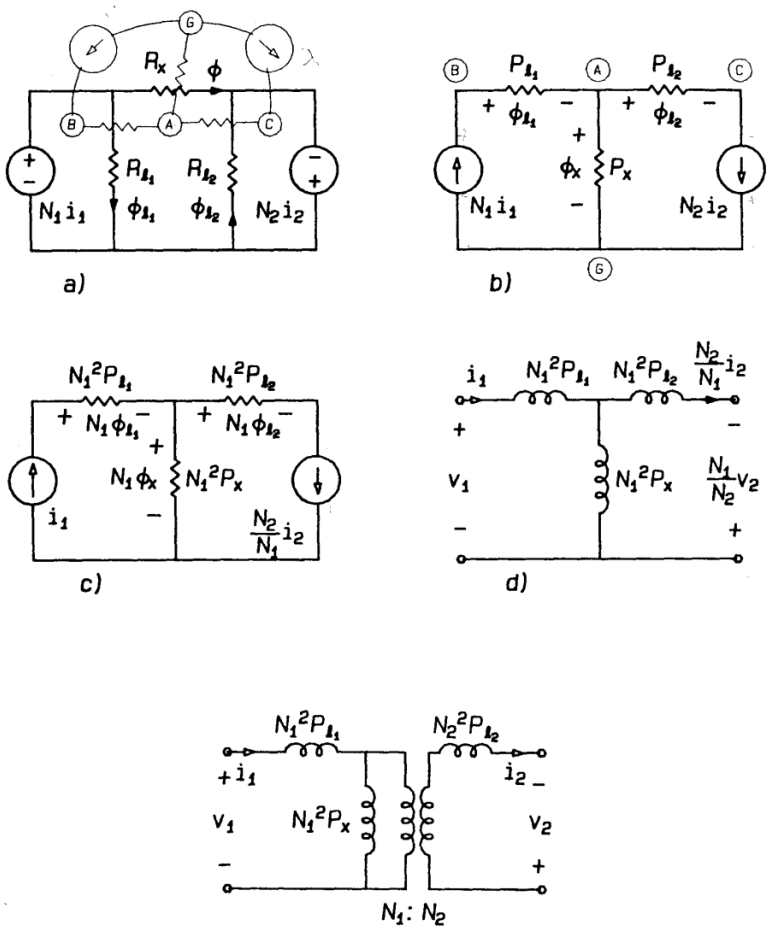

Figure A.1: Example explaining the principle of duality